Spin decoherence of InAs surface electrons by transition metal ions

Yao Zhang, V. Soghomonian, and J. J. Heremans

Phys. Rev. B **97**, 155439 — Published 30 April 2018

DOI: 10.1103/PhysRevB.97.155439

Spin decoherence of InAs surface electrons by transition metal ions

Yao Zhang,[1] V. Soghomonian,[1] and J. J. Heremans[1,*]

[1]*Department of Physics, Virginia Tech, Blacksburg, Virginia 24061, USA*

(Dated: April 17, 2018)

Spin interactions between a two-dimensional electron system at the InAs surface and transition metal ions, Fe^{3+}, Co^{2+} and Ni^{2+}, deposited on the InAs surface, are probed by antilocalization measurements. The spin-dependent quantum interference phenomena underlying the quantum transport phenomenon of antilocalization render the technique sensitive to the spin states of the transition metal ions on the surface. The experiments yield data on the magnitude and temperature dependence of the electrons' inelastic scattering rates, spin-orbit scattering rates, and magnetic spin-flip rates as influenced by Fe^{3+}, Co^{2+} and Ni^{2+}. A high magnetic spin-flip rate is shown to mask the effects of spin-orbit interaction, while the spin-flip rate is shown to scale with the effective magnetic moment of the surface species. The spin-flip rates and their dependence on temperature yield information about the spin states of the transition metal ions at the surface, and in the case of Co^{2+} suggest either a spin transition or formation of a spin-glass system.

PACS numbers: cfr. Physics Subject Headings

INTRODUCTION

One of the central and common concepts to magnetism, spin physics and spin-based technologies lies in the spin-exchange interactions between carriers and local moments. In the present work, spin-sensitive transport-based quantum interference experiments are used to study spin interactions between transition metal (TM) ions (Fe^{3+}, Co^{2+} and Ni^{2+}) on the surface of (001) InAs and a two-dimensional electron system (2DES) accumulated in close proximity at the same surface. Investigations of surface magnetism and its interactions with carriers in a thin-film host have likewise attracted attention [1–8]. The TM ions modify the spin-flip scattering rate and the spin-orbit interaction (SOI) properties of the 2DES electrons, in turn modifying the quantum phase coherence properties in the 2DES. The quantum coherence properties are in this work quantified by the weak-localization quantum coherence corrections to the conductivity of the 2DES, caused by interference between backscattered time-reversed electron trajectories. The quantum coherence corrections lead to a 2DES resistance R with a specific dependence on the magnetic field B applied normally to the surface, under strong SOI known as antilocalization (AL) [2–5, 9–11]. These quantum coherence corrections are a sensitive probe for the effects of magnetic impurities, capable of quantifying spin interactions [12, 13]. A parallel can be drawn with magnetic resonance methods (NMR, EPR), which also characterize a local spin environment by measuring a spin decoherence time (T_2). The 2DES magnetoresistance (MR) due to AL is determined by four characteristic decoherence or scattering rates (inverse scattering times) [2, 3, 5, 10, 14]: the elastic scattering rate τ_0^{-1} as deduced from the areal electron density N_S and mobility μ; the SOI scattering rate τ_{SO}^{-1}; the inelastic scattering rate τ_i^{-1}; and the magnetic spin-flip scattering rate τ_s^{-1}. The total electron decoherence rate τ_ϕ^{-1} is expressed [15, 16] as $\tau_\phi^{-1} = \tau_i^{-1} + 2\tau_s^{-1}$. Here τ_s^{-1} carries the information about the interactions between the TM surface local moments and the 2DES, and τ_{SO}^{-1} carries information about the SOI strength. Prominent SOI facilitates unique numerical fits of the AL model to the data because the characteristic MR of AL shows a turnaround from positive to negative MR under increasing B. The InAs surface 2DES has prominent Rashba SOI [2, 3, 17], and moreover provides electrons in close proximity to the local TM moments. The Fermi level E_F is at the surfaces of InAs pinned above the conduction band, forming a surface 2DES [2, 3, 18–21]. In recent experiments rare earth ions [2] and hemin [3] were deposited on the surface of InAs films to probe the spin interactions between surface electrons and the local magnetic species. While the rare earth ions possess large magnetic moments, the $4f$ shells responsible for paramagnetism of rare earth ions lie deep inside the $5s$ and $5p$ shells and as a result spin interactions with the itinerant electrons are partially screened. To study a system with reduced screening, in the present study TM ions are applied as magnetic surface species (MSS). The $3d$ shells responsible for ferromagnetism of TM ions are outermost, and strong interactions with InAs surface electrons are anticipated, borne out by the experiments described below.

EXPERIMENTAL METHODS

The MR measurements are performed by using standard four-contact low-frequency lock-in techniques. The experiment temperature T varies from 0.40 K to 6.0 K, maintained in a ^{3}He cryostat, with B applied perpendicularly to the sample surface. The sample consists of a 3.75 μm thick n-type (001) InAs film. Serpentine mesa structures (Fig. 1), fabricated on the InAs film via photolithography, are designed to enhance the MR signal by increasing channel length (8820 μm) to width (30 μm) ratio. The experiment is comparative, between before and after the deposition of MSS. Thus two neighboring mirror-twin serpentines are used, as shown in Fig. 1. For each experiment and sample, onto only one of the twin mesas the following MSS are deposited: Ni^{2+}, Co^{2+}, and Fe^{3+}. The TM ions are deposited from their respec-

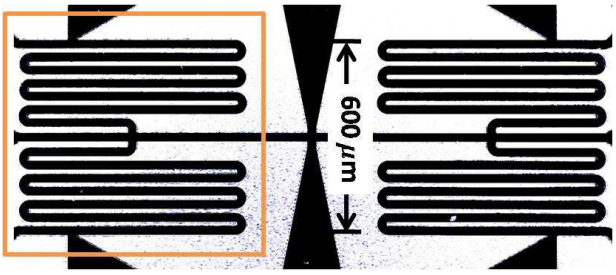

FIG. 1: Optical micrograph of a sample with two identical (001) InAs serpentine mesa patterns adjacent to each other (dark areas; in light areas the InAs is etched to the GaAs substrate). For comparative measurements, the left serpentine is covered by the surface species within the square outline and the right serpentine is kept bare.

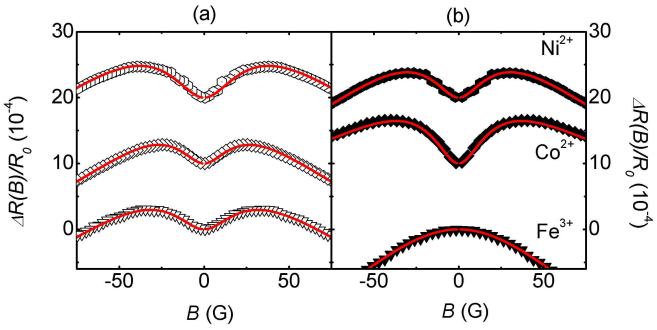

FIG. 2: (a) Magnetoresistance due to AL at 0.40 K on the bare serpentine mesas twinned with the Ni^{2+}(hexagons)-, Co^{2+}(diamonds)- and Fe^{3+}(down triangles)-covered serpentine mesas in (b). (b) Magnetoresistance due to AL at 0.40 K on the covered serpentine mesas twinned with the bare serpentine mesas in (a) (1 out of 6 experimental points are plotted, curves offset by 1.0×10^{-3}). Solid lines are theoretical fits ([23]).

tive nitrate salts, $Ni(H_2O)_6(NO_3)_2$, $Co(H_2O)_6(NO_3)_2$, and $Fe(H_2O)_6(NO_3)_3.3H_2O$, dissolved in aqueous solutions with a concentration of 6×10^{-4} M. A 0.01 μL of any solution is deposited and air-dried. The dried solutions leave a film with defined edges indicating an areal density of MSS on the order of 10^6 μm^{-2}. At the edge of the deposited area, higher MSS concentration may exist, however, no cluster formation is detected by atomic force microscopy, and the AL results form an average over the serpentine mesas. Therefore, the local variation of the areal density does not affect the AL signals. To verify that the measured differences in AL signal are due to the MSS only, the role of both deionized water and the nitrate anion were evaluated. Each serpentine mesa experiences a deionized water rinse as the final step of the fabrication process. Since the measurement consists of a comparison of the AL data between a bare (*i.e.* previously covered by deionized water) mesa and an MSS covered mesa, we can consider the contribution of deionized water and of possible oxidation to be eliminated. The influence of the nitrate anion on the AL signal was assessed by the comparative measurement of a bare mesa and a mesa covered with a $Bi(NO_3)_3.5H_2O$ solution of the same concentration. The Bi^{3+} ions have a spin angular momentum quantum number S=0, and thus any observed difference may be attributed to the nitrate ions. No significant difference was observed, indicating that contributions from nitrate anions or from possible oxidation do not impact the comparative AL measurements below [2]. Moreover, the twin serpentines are fabricated simultaneously on the same sample and experience the same cooldown, and hence the measured differences in AL signals will be due only to the presence of MSS and their interactions with the 2DES. The comparative (rather than absolute) data allows the analysis.

From magnetotransport measurements and $R(B=0)$, it is determined that the InAs surface 2DES has $N_S \sim 0.6\times10^{12}$ cm^{-2} and $\mu \sim 22,000$ cm^2/Vs at T = 0.40 K. N_S and μ are determined for each serpentine and for each T. The 2D diffusion constant D is calculated using the degenerate expression $D=\frac{1}{2}v_F^2\tau_0$, where v_F is the Fermi velocity derived from N_S (more details available in [2]). A possible positive correction to D due to spin polarization and concomitant Pauli blockade [22] is neglected, because the net spin polarization of the InAs 2DES due to the MSS is deemed small. For a given sample, N_S, μ and D do not vary in the range of the experimental T. While N_S, μ and D vary slightly among samples due to different cooldown history, no significant systematic variations are caused by solution coverage, which allows direct comparisons of the quantum properties among all serpentine mesas. The MR is presented as $\Delta R(B)=R(B)-R(B=0)$ normalized to $R_0=R(B=0)$, where R is the sample resistance. Inspection of Fig. 2, presented as an example obtained at T = 0.40 K, shows that AL signals are clearly changed by TM ions, indicating interactions between TM ions and the 2DES. The sharp positive MR for $B\sim0$, crossing over to negative MR at higher B, is characteristic for AL.

The quantum corrections to the 2D conductivity $\sigma_2(B)$ arising from AL are small. Since then $\Delta R(B) \ll R_0$, we linearize to $\Delta\sigma_2(B)/\sigma_2(B=0) \approx -\Delta R(B)/R_0$, with $\Delta\sigma_2(B)=\sigma_2(B)-\sigma_2(B=0)$, which allows direct comparison to experimental $R(B)$ values. To fit the data and extract τ_i^{-1}, τ_s^{-1}, and τ_{SO}^{-1}, this work uses an expression for $\Delta\sigma_2(B)$ from Ref. [10] modified to include spin-flip scattering [2, 3]:

$$\Delta\sigma_2(B)=\frac{e^2}{2\pi^2\hbar}\left\{-\left[\psi(\frac{1}{2}+\frac{B_0}{B})-\psi(\frac{1}{2}+\frac{B_i+B_{SO}+B_s}{B})+\frac{1}{2}\psi(\frac{1}{2}+\frac{B_i+2B_s}{B})-\frac{1}{2}\psi(\frac{1}{2}+\frac{B_i+2B_{SO}}{B})\right]\right.$$
$$\left.+\left[ln(\frac{B_0}{B})-ln(\frac{B_i+B_{SO}+B_s}{B})+\frac{1}{2}ln(\frac{B_i+2B_s}{B})-\frac{1}{2}ln\left(\frac{B_i+2B_{SO}}{B}\right)\right]\right\} \quad (1)$$

where $\psi(x)$ is the digamma function and each scattering time τ_α (with $\alpha = 0, i, SO, s$) corresponds to a characteristic magnetic field $B_\alpha = \hbar/(4eD\tau_\alpha)$. B_i, B_{SO} and B_s are used as fitting parameters allowing the determination of τ_i, τ_{SO} and τ_s, while B_0 is independently known from τ_0 for all serpentine mesas. The MR measurement of the bare serpentine determines B_i and B_{SO} when spin-flip scattering is absent ($\tau_s \to \infty$). By assuming τ_i unchanged in the presence of MSS [4], B_i, B_{SO} and B_s of the serpentine bearing the MSS can then be determined after fitting the corresponding MR measurement, and τ_i, τ_{SO} and τ_s are obtained in the presence of MSS [2, 3]. The experimental data follow Eq. (1) to good precision, as observed in the example of Fig. 2, while also resulting in a consistent series of scattering rates τ_α^{-1} compatible with physical understanding.

RESULTS AND DISCUSSION

A comparison between Fig. 2a and Fig. 2b demonstrates the sensitivity of AL to MSS. Coverage with Ni^{2+} reduces the sharp positive MR for $B \sim 0$ characteristic for AL, and coverage with Fe^{3+} changes the AL signal into a weak-localization signal characteristically entirely lacking the positive MR for $B \sim 0$. Both Ni^{2+} and Fe^{3+}, and particularly the latter, hence mask the observation of the SOI responsible for AL. This observation may be explained by considering suppression of SOI due to ferromagnetic ordering on the surface [24, 25]. Alternatively, the high τ_s^{-1} induced by Ni^{2+} and Fe^{3+} may cause fast spin dephasing and thus mask SOI. Indeed SOI locks spin to momentum while maintaining spin phase, whereas spin-flip scattering randomizes the spin phase. In Eq. (1) the terms with B_i, B_{SO} and B_s can be expressed in 2 combinations, namely $B_i + 2B_s$ corresponding to B_ϕ, and $B_{SO} - B_s$. Correspondingly, τ_{SO}^{-1} and τ_s^{-1} occur as $\tau_{SO}^{-1} - \tau_s^{-1}$, showing that the two scattering mechanisms indeed oppositely influence the spin decoherence measured by AL. Spin-flip scattering can then change the MR signal from AL characteristic of substantial SOI, to weak-localization, characteristic of weakened or screened SOI. These qualitative observations will be detailed below, as will be the effect of coverage with Co^{2+}.

The observed AL signal is influenced by the electron configuration and symmetry of the TM complexes on the surface. The $3d$ electron configurations of the TM ions correspond to d^5 for Fe^{3+}, d^7 for Co^{2+} and d^8 for Ni^{2+}. The TM ions are deposited from their aqueous nitrate salt solutions, where each TM center is in an octahedral geometry coordinated to 6 H_2O molecules, and associated with nitrate anions for charge balance. Compared to the 5 degenerate $3d$ orbitals for a free ion, in an octahedral geometry the $3d$ energy levels form 3 t_{2g} and 2 e_g levels due to crystal field splitting, as shown in Fig. 3. The energy separation between the t_{2g} and e_g levels is related to the TM and the surrounding ligands, here all H_2O. The schematic in Fig. 3 shows different energy separations, and is calculated setting the energy difference in the case of the Ni^{2+} complex as 1 unit [26]. Indicated in the middle

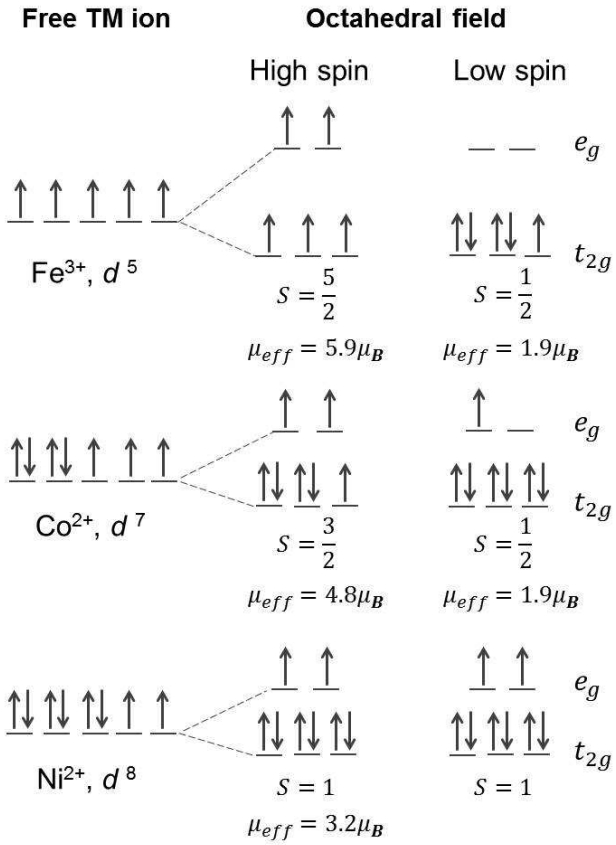

FIG. 3: Comparison of the electron configurations of the free (left column), high-spin (middle column) and low-spin (right column) states of the 3 TM ions studied. In each case, the total spin S of the state and the associated effective magnetic moments are indicated.

column of Fig. 3 are TM ions in perfect octahedral geometry with 6 identical H_2O ligands favorable to forming high-spin complexes. In the right column, low-spin configurations are shown, and in all cases the total spin S is indicated, as well as representative values for the observed effective magnetic moments $\mu_{\rm eff}$ expressed in Bohr magnetons μ_B. In the low-spin cases for Fe^{3+} and Co^{2+}, $\mu_{\rm eff}$ is essentially that of a single unpaired electron [27]. In the d^8 Ni^{2+} system, the electron configuration of the high- and low-spin cases is identical, and forms the baseline for our comparative discussion.

The dependence on T of τ_i^{-1} for all TM samples is presented in Fig. 4. The TM samples show a linear dependence on T of τ_i^{-1}, consistent with Nyquist decoherence arising from fluctuations in the electromagnetic background [2, 3, 14, 28–30]. The comparison in Fig. 5 between τ_{SO}^{-1} for bare *vs* MSS-covered serpentine mesas demonstrates that τ_{SO}^{-1} and hence SOI increase in the presence of TM ions, negating the formation of a ferromagnetic surface ordering as an explanation for the reduction of the AL signals. The increase in SOI may be attributed to the interaction of the electric fields produced by the surface TM ions with the 2DES [11, 17, 23]. Inspection of Fig. 5 indicates the greatest change in the case

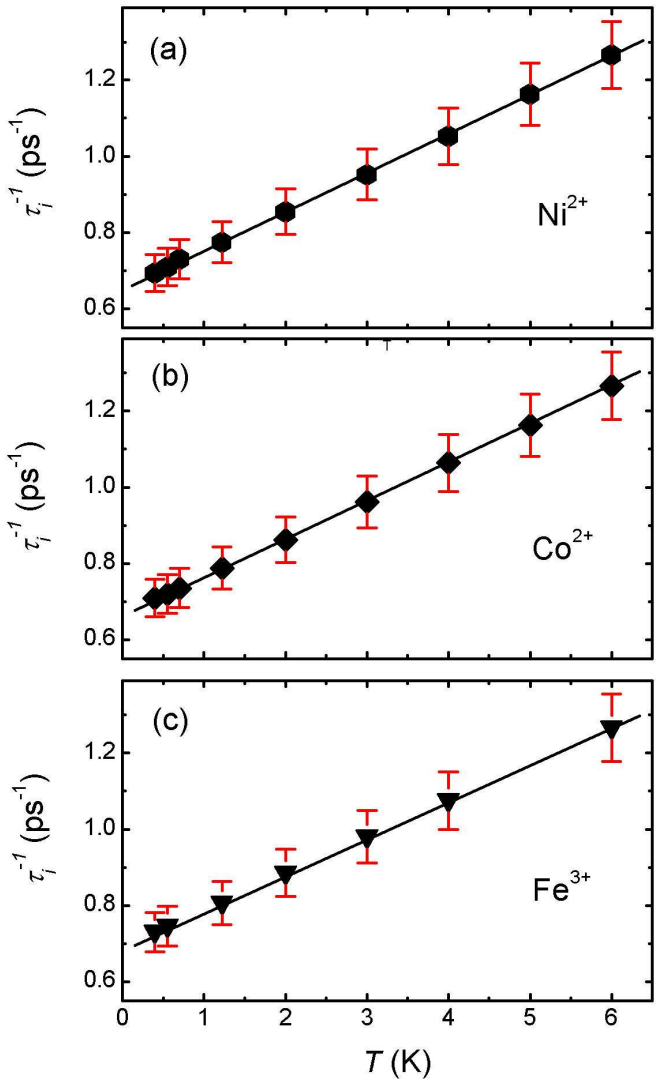

FIG. 4: Inelastic scattering rates τ_i^{-1} *vs* T for (a) Ni^{2+}(hexagons)-covered mesas; (b) Co^{2+}(diamonds)-covered mesas; (c) Fe^{3+}(down triangles)-covered mesas. The ion-covered and bare mesas share the same value, thus values for bare mesas are omitted. Solid lines form guides to the eye. Error bars are indicated.

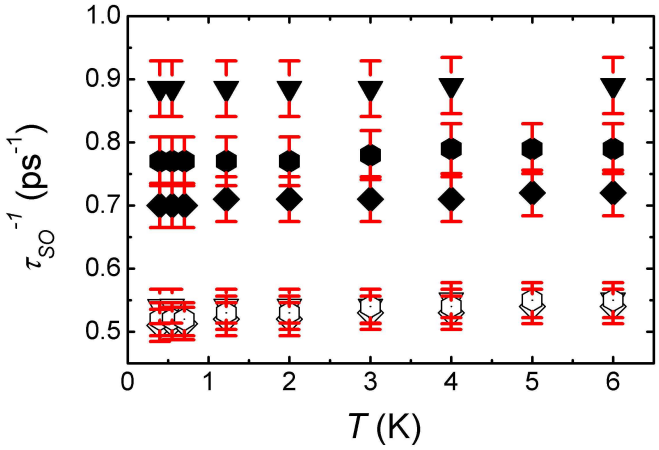

FIG. 5: Spin-orbit scattering rates τ_{SO}^{-1} *vs* T for the Ni^{2+}(hexagons)-covered mesas, the Co^{2+}(diamonds)-covered mesas, and the Fe^{3+}(down triangles)-covered mesas. Solid symbols represent data for ion-covered mesas while open symbols represent data for bare mesas. Error bars are indicated.

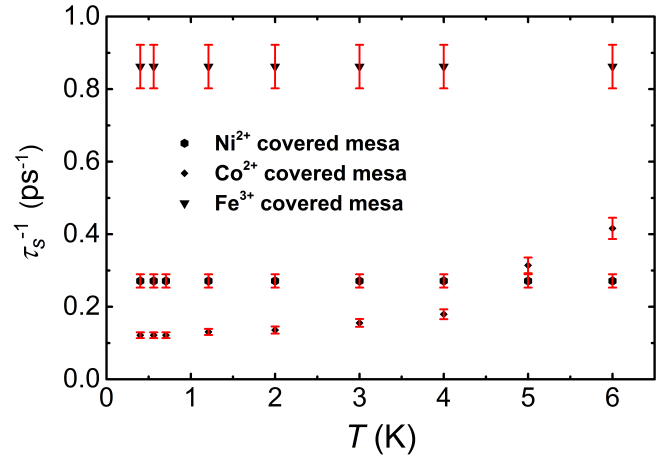

FIG. 6: Magnetic spin-flip rates τ_s^{-1} *vs* T, measured on the mesas covered with *resp.* Ni^{2+}(hexagons), Co^{2+}(diamonds), or Fe^{3+}(down triangles). Error bars are indicated.

of the Fe^{3+} with +3 oxidation state, with lesser effects from Ni^{2+} and Co^{2+}, both with +2 oxidation state, supporting the reasoning. With all three TMs, τ_{SO}^{-1} remains approximately constant with T within the range of T in the study. However, Fig. 6 shows that magnetic spin-flip scattering, quantified by τ_s^{-1}, by only Ni^{2+} and Fe^{3+} remain approximately constant within the same range of T, while magnetic spin-flip scattering by Co^{2+} increases as a function of T, albeit not linearly and with a saturation of τ_s^{-1} visible below 2 K.

We begin the discussion of the scattering rates by defining the difference in spin-orbit scattering between bare ($\tau_{SO}^{-1}|_{bare}$) and MSS-covered ($\tau_{SO}^{-1}|_{cov}$) serpentine mesas, and the difference of spin-flip scattering between bare ($\tau_s^{-1}|_{bare} = 0$) and MSS-covered ($\tau_s^{-1}|_{cov} = \tau_s^{-1}$) serpentine mesas, as:

$$\begin{aligned} \Delta\tau_{SO}^{-1} &= \tau_{SO}^{-1}|_{cov} - \tau_{SO}^{-1}|_{bare}, \\ \Delta\tau_s^{-1} &= \tau_s^{-1}|_{cov} - \tau_s^{-1}|_{bare} = \tau_s^{-1}. \end{aligned} \tag{2}$$

A positive $\Delta\tau_{SO}^{-1}$ leads to more pronounced AL. However, as mentioned, with increasing $\Delta\tau_s^{-1}$ the spin flips disturb the spin phase and hence disturb the spin quantum interference leading to AL, and thereby mask the effect of SOI. Increasing $\Delta\tau_{SO}^{-1}$ broadens and deepens the MR trace characteristic of AL, while increasing $\Delta\tau_s^{-1}$ tends to weaken the positive MR and leads to an MR characteristic of weak-localization. From Fig. 5, $\Delta\tau_s^{-1} = \tau_s^{-1}$ increases according to the sequence Co^{2+} (low) $\rightarrow$ Ni^{2+} $\rightarrow$ Fe^{3+} (high). The ratios of $\Delta\tau_s^{-1}/\Delta\tau_{SO}^{-1}$ at T = 0.40 K are 2.5, 1.1, and 0.5 for the Fe^{3+}, Ni^{2+}, and Co^{2+} MSS respectively. For

Fe^{3+} MSS, Fig. 2 shows that the AL signal changes to weak-localization, indicating that the spin-flip scattering indeed influences this sample the most, in accordance with the highest ratio $\Delta\tau_s^{-1}/\Delta\tau_{SO}^{-1}$. With the Ni^{2+} and Co^{2+} MSS the effects of SOI are less suppressed, inferred from the observation that the AL signals in these two cases do not change to weak-localization. Yet, with the Ni^{2+} MSS the MR trace is narrowed and lowered while for the Co^{2+} sample it is broadened and deepened, indicating that a threshold between appearance of AL or weak-localization occurs for $0.5 \leq \Delta\tau_s^{-1}/\Delta\tau_{SO}^{-1} \leq 1.1$.

The spin-flip scattering is related to $\mu_{\rm eff}$ of the TM ion, in turn related to the high- or low-spin state of the ion, with increasing τ_s^{-1} expected to correlate with increasing $\mu_{\rm eff}$ [2, 3]. For Fe^{3+} and Co^{2+}, a high- and low-spin state are possible. The high-spin to low-spin $\mu_{\rm eff}$ then range for Fe^{3+} from 5.9 μ_B to 1.9 μ_B and for Co^{2+} from 4.8 μ_B to 1.9 μ_B. For Ni^{2+} no difference exists between high- and low-spin states, both with $\mu_{\rm eff}$ = 3.2 μ_B. Concerning τ_s^{-1} we thus compare the Fe^{3+} and Co^{2+} MSS data to the Ni^{2+} MSS data. As indicated in Fig. 6, the data on τ_s^{-1} supports the high-spin state for Fe^{3+} , where moreover this spin state appears not to change over T. If Co^{2+} resided in its high-spin state, then τ_s^{-1} with Co^{2+} MSS should lie close to τ_s^{-1} with Fe^{3+} MSS. Yet inspection of Fig. 6 shows that τ_s^{-1} with Co^{2+} MSS lies close to τ_s^{-1} with Ni^{2+} MSS, hinting to a mixed but mostly low-spin state at the lowest T = 0.40 K for Co^{2+}. Moreover for Co^{2+}, τ_s^{-1} increases with increasing T, and at T = 6.0 K τ_s^{-1} for Co^{2+} exceeds τ_s^{-1} for Ni^{2+} while remaining below τ_s^{-1} for Fe^{3+}, again hinting to a change with T in the spin state of the Co^{2+} MSS. We note that $\mu_{\rm eff}$ of Ni^{2+} is $\sim$ the average of the high- and low-spin $\mu_{\rm eff}$ of Co^{2+}. Thereby, when most of the Co^{2+} ions complete the spin transition from low to high, the value of τ_s^{-1} for the Co^{2+}-covered mesa is anticipated to be $\tau_s^{-1}(Co^{2+})|_{\rm high-spin} \sim 2\tau_s^{-1}(Ni^{2+}) - \tau_s^{-1}(Co^{2+})|_{\rm low-spin} = 0.42$ ps^{-1} if a linear relation between $\mu_{\rm eff}$ and τ_s^{-1} is assumed. From Fig. 6, $\tau_s^{-1}(Co^{2+})$ = 0.41 ps^{-1} at T = 6.0 K, strongly suggesting a spin crossover process. Considering a spin crossover in the case of Co^{2+}, we assume that as T is increased, the proportion of high-spin to low-spin Co^{2+} in the population increases according to a spin crossover process that is driven by T (as opposed to pressure- or B-driven). The mole fraction function $\rho_H(T)$ of Co^{2+} ions in their high-spin state can then be written as:

$$\rho_H(T) = \frac{1}{e^{\alpha(T_{1/2}-T)}+1}, \qquad (3)$$

where the inverse of the heuristic fitting parameter α denotes a temperature scale proportional to the energy required to promote electrons from the t_{2g} to the e_g level and convert low-spin Co^{2+} to high-spin Co^{2+}. The $T_{1/2}$ denotes the temperature for a coexistence of 50% of low-spin and 50% of high-spin Co^{2+} ions. We can obtain the expression for the T dependence of the spin-flip rate of the Co^{2+}-covered mesa as (adapted from Ref. [31]):

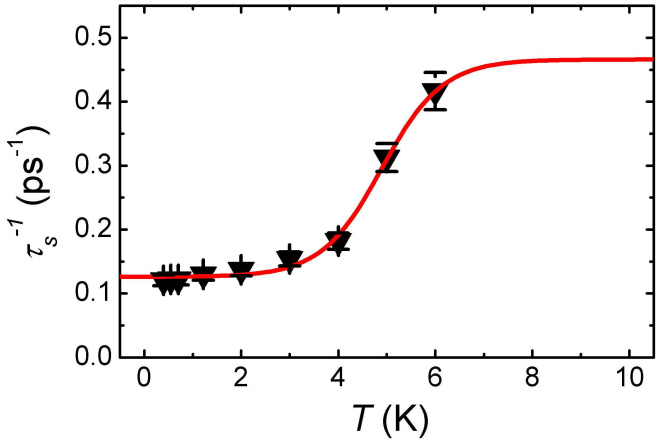

FIG. 7: Data and modeling of τ_s^{-1} *vs* T for the Co^{2+}-covered mesas. Down triangles represent experimental data, with error bars indicated. The red solid line represents a theoretical fit as explained in the text.

$$\tau_s^{-1}(T) = \tau_s^{-1}|_{\rm low-spin} + \Delta\tau_{s,H-L}^{-1}\rho_H(T), \qquad (4)$$

where $\Delta\tau_{s,H-L}^{-1} = \tau_s^{-1}|_{\rm high-spin} - \tau_s^{-1}|_{\rm low-spin}$.

Figure 7 demonstrates the fitting result of applying Eq. 4 to simulate the spin-flip rate data of the Co^{2+}-covered mesa. From the fitting α, $T_{1/2}$, $\tau_s^{-1}|_{\rm low-spin}$, and $\Delta\tau_s^{-1}$ are derived to be 1.6 K^{-1}, 4.9 K, 0.13 ps^{-1}, and 0.34 ps^{-1}. Accordingly, the spin-flip rate in high-spin state is 0.47 s^{-1}, consistent with the expectation of $\tau_s^{-1}(Co^{2+})|_{\rm high-spin} = 0.42$ ps^{-1} and the observed spin-flip rate of Co^{2+} of 0.41 ps^{-1} at 6.0 K. The agreement between experimental data and the theoretical calculation suggests the existence of a spin transition. Data for $T > 6$ K for Fig. 7 cannot be obtained using the AL approach as quantum coherence is lost at higher T and the AL signal vanishes.

Knowing that at low T Fe^{3+} is in its high-spin state and Co^{2+} is in its low-spin state, the S, L and J of these TM ions in their ground state can be then determined following Hund's rules: Ni^{2+} has S = 1, L = 3 and J = 4; Co^{2+} has $S = \frac{1}{2}$, L = 4 and $J = \frac{9}{2}$; Fe^{3+} has $S = \frac{5}{2}$, L = 0 and $J = \frac{5}{2}$. Unlike the $4f$ electrons (deep inside the $5s$ and $5p$ shells) responsible for paramagnetism in rare earth ions, the $3d$ electrons of the TM ions reside in the outermost shell, and are thus unlikely to result in paramagnetism. Paramagnetic behavior may be observed in ferromagnetic or antiferromagnetic materials above their Curie temperature T_C, where thermal energy overcomes the interaction between the neighboring spins. However, the T_Cs of the MSS studied here are expected to much exceed our highest T = 6.0 K. Consequently, we rule out the presence of a paramagnetic system as a potential explanation for the T dependence of τ_s^{-1} in the case of Co^{2+} MSS.

In the following, the possibility is explored of spin-glass formation in the Co^{2+} MSS system as an explanation for the T dependence of τ_s^{-1} in the case of Co^{2+} MSS. The magnetic moments of the TM ions can be locked to specific orien-

tations by interaction with the substrate atoms or by RKKY interactions [6, 7, 32, 33], leading to a spin-glass system, which in turn reduces the spin-flip rate τ_s^{-1} compared to a free-spin system. Spin-glasses can occur where the axes of the magnetic moments are distributed isotropically (Heisenberg spin-glass), or are aligned parallel or antiparallel (Ising spin-glass). Under the present case of strong spin-orbit scattering ($\tau_{SO}^{-1} \gtrsim \tau_i^{-1}$), alignment of spins due to either type of spin-glasses are predicted to lead to the same reduction in τ_s^{-1} by a factor $S/(S+1)$ relative to the free-spin case [33, 34]. A smaller S thereby leads to stronger reduction of τ_s^{-1}. For Co^{2+} MSS we have $S = \frac{1}{2}$. Starting from an assumed free-spin state at T = 6.0 K to reach a spin-glass by T = 0.40 K would lead to a substantial reduction of τ_s^{-1} by a factor of 1/3 on cooling from 6.0 K to 0.40 K. From Fig. 6 in the case of Co^{2+} MSS, a saturation in $\tau_s^{-1} = 0.13\,\text{ps}^{-1}$ is observed when $T < 2$ K, compatible with alignment due to spin-glass formation below 2 K. As T increases a free-spin case develops, and starting from $\tau_s^{-1} = 0.13\,\text{ps}^{-1}$ at 2.0 K we find that the free-spin state should be characterized by $\tau_s^{-1} = ((S+1)/S)\,0.13$ ps^{-1} = 0.39 ps^{-1}. This value is consistent with $\tau_s^{-1} = 0.41$ ps^{-1} at T = 6.0 K in Fig. 6. Another saturation of τ_s^{-1} is then anticipated above 6 K, demonstrated also by the differently-derived fitting curve in Fig. 7. Experimentally the AL signal fades for $T > 6$ K and performing experiments at higher T does not yield a sufficient signal to extract information. Yet, the consistency between the spin-glass model and the experimental data of τ_s^{-1} suggests that spin-glass formation should not be excluded as explanation for the T dependence of τ_s^{-1} in the case of Co^{2+} MSS.

As an explanation for the increase with T of τ_s^{-1} in the case of Co^{2+} MSS (Fig. 6), we also explore formation of a Kondo system between the Co^{2+} MSS as local moments and the itinerant electrons in the InAs 2DES. In Kondo systems, a spin-singlet state is formed from single Kondo impurity and surrounding electrons within a Kondo cloud. Spin-flip scattering is increasingly suppressed as T is lowered below the Kondo temperature T_K, due to screening of the moment of the magnetic Kondo impurity by the electrons, and τ_s^{-1} reaches a maximum at T_K [2, 4, 13, 15, 35]. Since Fig. 6 shows that τ_s^{-1} is still increasing at T = 6.0 K (the highest T), for the present Co^{2+}/InAs system a $T_K > 6$ K could be deduced if a Kondo system were indeed formed. T_K for Co on Cu surfaces has been experimentally estimated at a relatively high $T_K \sim 60$ K [36–38]. Yet, for the InAs system, the low electron density compared to Cu will lower T_K substantially. The SOI in InAs and the dense MSS coverage will further depress T_K. For the Co^{2+}/InAs system, $T_K > 6$ K is hence unlikely. While the formation of a Kondo system cannot be excluded, it therefore appears as an unlikely explanation for the increase with T of τ_s^{-1} in the case of Co^{2+} MSS (Fig. 6).

Since both the present quantum interference method and NMR use spin decoherence times to detect magnetic moments, a qualitative sensitivity comparison between the approaches yields interesting insights. As pointed out by Ref. [12] (*cfr* also Ref. [5]), the quantum interference method based on AL can readily detect $\sim \frac{1}{1000}$ of a monolayer coverage of MSS. In NMR the signal-to-noise ratio linearly depends on the total magnetic moment of the sample and on the resonant frequency. In the AL approach however, the signal-to-noise ratio depends on the 2D length-to-width ratio and resistivity of the detecting area (together forming a resistance) and on the MSS coverage in the detecting area. The AL approach further has no dependence on a resonant frequency. Given a minimum detectable coverage of $\sim \frac{1}{1000}$ monolayer, the sensitivity of the AL approach does not directly depend on the total detecting area or hence total magnetic moment of the sample, but rather on the 2D length-to-width ratio of the detecting area. A small detecting area (*e.g.* a few μm^2, still sufficiently large to support diffusive electron transport) can hence lead to a sensitivity far surpassing NMR sensitivities. NMR and the AL approach will of course find applicability in elucidating different questions.

CONCLUSIONS

In a two-dimensional electron system on InAs, quantum interference measurements in the form of antilocalization were used to quantify the spin interactions between the low-dimensional electron system and local moments from transition metal ions Fe^{3+}, Co^{2+} and Ni^{2+} deposited in close proximity on the InAs surface. The use of antilocalization as a probe of electron spin decoherence allows measurements akin to magnetic resonance techniques. The measurements reveal the magnitude and temperature dependence of inelastic scattering rate, the spin-orbit scattering rate, and the magnetic spin-flip rate of the InAs surface electrons as modified by the different transition metal ions. The experiments show that a high magnetic spin-flip rate can mask the effects of spin-orbit interaction and that the spin-flip rate scales with the effective magnetic moment of the surface species. The experiments also show that the spin-flip rates and their dependence on temperature can be used to deduce information about the spin states of the transition metal ions at the surface.

ACKNOWLEDGMENTS

The work was supported by the U.S. Department of Energy, Office of Basic Energy Sciences, Division of Materials Sciences and Engineering under award DOE DE-FG02-08ER46532.

* Electronic address: heremans@vt.edu; Author to whom correspondence should be addressed: Department of Physics, Virginia Tech, Blacksburg, VA 24061, USA

[1] C. Weeks, J. Hu, J. Alicea, M. Franz, and R. Wu, Phys. Rev. X **1**, 021001 (2011).

[2] Yao Zhang, R. L. Kallaher, V. Soghomonian, and J. J. Heremans, Phys. Rev. B **87**, 054430 (2013).

[3] V. Deo, Yao Zhang, V. Soghomonian, and J. J. Heremans, Scientific Reports 5:9487 (2015) DOI: 10.1038/srep09487.

[4] W. Wei, and G. Bergmann, Phys. Rev. B **37**, 5990 (1988).

[5] G. Bergmann, Int. J. Mod. Phys. B **24**, 2015 (2010).

[6] J. J. Zhu, D.X. Yao, S. C. Zhang, and K. Chang, Phys. Rev. Lett. **106**, 097201 (2011).

[7] L. Zhou, J. Wiebe, S. Lounis, E. Vedmedenko, F. Meier, S. Blügel, P.H. Dederichs, and R. Wiesendanger, Nat. Phys. **6**, 187 (2010).

[8] T. Gang, M. Deniz Yilmaz, D. Atac, S. K. Bose, E. Strambini, A. H. Velders, M. P. de Jong, J. Huskens, and W. G. van der Wiel, Nat. Nanotechnol. **7**, 232 (2012).

[9] G. Bergmann, Phys. Rep. **107**, 1 (1984).

[10] S. Hikami, A. I. Larkin, and Y. Nagaoka, Prog. Theor. Phys. **63**, 707 (1980).

[11] S. McPhail, C. E. Yasin, A. R. Hamilton, M. Y. Simmons, E. H. Linfield, M. Pepper, and D. A. Ritchie, Phys. Rev. B **70**, 245311 (2004).

[12] R. Schäfer, and G. Bergmann, Solid State Comm. **98**, 45 (1996).

[13] F. Mallet, J. Ericsson, D. Mailly, S. Ünlübayir, D. Reuter, A. Melnikov, A. D. Wieck, T. Micklitz, A. Rosch, T. A. Costi, L. Saminadayar, and C. Bäuerle, Phys. Rev. Lett. **97**, 226804 (2006).

[14] J. J. Lin, and J. P. Bird, J. Phys.: Condens. Matter **14**, R501 (2002).

[15] C. Van Haesendonck, J. Vranken, and Y. Bruynseraede, Phys. Rev. Lett. **58**, 1968 (1987).

[16] J. C. Licini, G. J. Dolan, and D. J. Bishop, Phys. Rev. Lett. **54**, 1585 (1985).

[17] C. Schierholz, T. Matsuyama, U. Merkt, and G. Meier, Phys. Rev. B **70**, 233311 (2004).

[18] D. C. Tsui, Phys. Rev. B **12**, 5739 (1975).

[19] T. Mochizuki, R. Masutomi, and T. Okamoto, Phys. Rev. Lett. **101**, 267204 (2008).

[20] M. Noguchi, K. Hirakawa, and T. Ikoma, Phys. Rev. Lett. **66**, 2243 (1991).

[21] L. F. J. Piper, T. D. Veal, M. J. Lowe, and C. F. McConville, Phys. Rev. B **73**, 195321 (2006).

[22] F. Cadiz, D. Paget, and A. C. H. Rowe, Phys. Rev. Lett. **111**, 246601 (2013).

[23] Yao Zhang, and J. J. Heremans, Solid State Communications **177**, 36 (2014).

[24] M. M. Glazov, E. Ya. Sherman, and V. K. Dugaev, Physica E **42**, 2157 (2010).

[25] V. K. Dugaev, P. Bruno, and J. Barnas, Phys. Rev. B **64**, 144423 (2001).

[26] T. M. Dunn, D. S. McClure and R. G. Pearson, Some Aspects of Crystal Field Theory, Harper and Row, New York (1965).

[27] B. N. Figgis and J. Lewis, Progr. Inorg. Chem. **6**, 37 (1964).

[28] B. L. Altshuler, A.G. Aronov, and D.E. Khmelnitsky, J. Phys. C: Solid State Phys. **15**, 7367 (1982).

[29] R. L. Kallaher, and J. J. Heremans, Phys. Rev. B **79**, 075322 (2009).

[30] Y. Xie, C. Le Priol, and J. J. Heremans, J. Phys.: Condens. Matter **28**, 495003 (2016).

[31] C. P. Slichter, and H. G. Drickamer, J. Chem. Phys. **56**, 2142 (1972).

[32] M. A. Ruderman, and C. Kittel, Phys. Rev. **96**, 99 (1954).

[33] W. Wei, G. Bergmann, and R. P. Peters, Phys. Rev. B **38**, 11751 (1988).

[34] R. P. Peters, G. Bergmann, and R. M. Mueller, Phys. Rev. Lett. **60**, 1093 (1988).

[35] G. M. Alzoubi, and N. O. Birge, Phys. Rev. Lett. **97**, 226803 (2006).

[36] N. Néel, J. Kröger, R. Berndt, T. O. Wehling, A. I. Lichtenstein, and M. I. Katsnelson, Phys. Rev. Lett. **101**, 266803 (2008).

[37] N. Knorr, M. A. Schneider, L. Diekhöner, P. Wahl, and K. Kern, Phys. Rev. Lett. **88**, 096804 (2002).

[38] B. Surer, M. Troyer, P. Werner, T. O. Wehling, A. M. Läuchli, A. Wilhelm, and A. I. Lichtenstein, Phys. Rev. B **85**, 085114 (2012).